

Depth imaging using slowness-averaged Kirchhoff extrapolators

Hugh D. Geiger, Gary F. Margrave, Kun Liu, Pat F. Daley

ABSTRACT

Recursive Kirchhoff wavefield extrapolation in the space-frequency domain can be thought of as a simple convolutional filter that calculates a single output point at depth $z+dz$ using a weighted summation of all input points within the extrapolator aperture at depth z . The desired velocity values for the extrapolator are the ones that provide the best approximation of the true phase (propagation time) of the seismic wavefield between the input points and the output point. Recursive Kirchhoff extrapolators can be designed to handle lateral variations in velocity in a number of ways: a PSPI-type extrapolator uses only the velocity at the output point, a NSPS-type extrapolator uses the velocities at the input points; a SNPS-type extrapolator incorporates two extrapolation steps of $dz/2$ where the first step uses the velocities at the input points (NSPS-type) and the second step uses the velocity at the output point (PSPI-type); while the Weyl-type extrapolator uses an average of the velocities between each input point and the output point. Here, we introduce the PAVG-type extrapolator, which uses velocity values calculated by an average of slowness along straight raypaths between each input point and the output point. A simple synthetic with a lateral step in velocity shows that the PAVG Kirchhoff extrapolator is very close to the exact desired response. Tests using the Marmousi synthetic data set suggest that the extrapolator behaviour is only one of many considerations that must be addressed for accurate depth imaging. Other important considerations include preprocessing, aperture size, taper width, and imaging condition.

INTRODUCTION

Prestack ‘wave equation’ depth imaging can be implemented as a shot-record migration, which combines recursive forward and backward wavefield extrapolation with an imaging condition (Figure 1). In shot-record migration, the recorded shot record is downward continued into the subsurface by backward wavefield extrapolation, a modelled shot is downward continued into the subsurface by forward wavefield extrapolation, and an image consisting of bandlimited estimates of subsurface reflectivity is extracted from the wavefields at each depth level. Kirchhoff extrapolators are implemented as a convolutional filter relating input points on one depth level to output points on the next depth level (Figure 2). Because the extrapolators do not vary with time, they can be implemented efficiently in the space-frequency domain.

In a previous paper, we developed the theory of recursive Kirchhoff wavefield extrapolators (Margrave and Daley, 2001). Only a brief summary of the theory will be repeated here. Beginning with the Fourier integral operator expressions for the wavefield extrapolators: GPSPI (*generalized phase shift plus interpolation*), NSPS (*nonstationary phase shift*), and the Weyl operator (based upon a quantum mechanical idea in Weyl (1931)) (see Margrave and Ferguson, 1998, 1999, and Ferguson and Margrave 2001), expressions were derived for these three extrapolators in the space-frequency domain. An additional extrapolator - SNPS (*symmetric nonstationary phase shift*) - can be developed as a cascade of NSPS and GPSPI. As might be expected, these expressions turned out to

be Kirchhoff-style operators that accomplish a single wavefield extrapolation step rather than a complete migration. The only difference between the four operators, NSPS, GPSPI, SNPS, and Weyl, was found to be in the way they handle velocity. In papers that followed (Geiger et al. 2002; Margrave and Geiger, 2002), we applied Kirchhoff extrapolators to parallel 3D prestack depth imaging and to the extrapolation of poorly sampled wavefields acquired on surfaces with topography.

For wavefield extrapolators, accuracy in phase is generally more important than accuracy in amplitude. The accumulated traveltimes (or phase) along a path between a given input point and an output point is the integrated slowness. Our previous Kirchhoff extrapolators used only the velocities at the input or output points for the convolutional filter. A natural extension is to include the velocities at intermediate points, and average their slowness to achieve a better estimate of phase. In this paper, we introduce the PAVG or slowness averaged Kirchhoff extrapolator. The PAVG extrapolator is ideally suited to implementation in the space-frequency domain. For true-amplitude or relative-amplitude-preserving imaging, the extrapolator is only one of a number of important considerations that can affect the accuracy of the final image. We also examine shot-record preprocessing, source wavefield modelling, and the migration imaging condition. Finite difference modeling is used to gain insight into how these considerations might best be addressed. The best solutions are combined to create an image of the shallow portion of the Marmousi dataset, and in particular, to compare and evaluate the PAVG, PSPI and tapered PAVG Kirchhoff extrapolators.

Recently, an alternate extrapolator scheme that takes advantage of average slowness has been proposed by Xu et al. (2003). They use a velocity adaptive coordinate transform (VACT) to remap the input data at each extrapolation step to new lateral coordinates with spacing proportional to a ratio of slowness over reference slowness. In the VACT domain, the classical constant-slowness phase-shift algorithm (Gazdag, 1978) can be efficiently applied to accurately extrapolate the data without dip limitation. An inverse-VACT is then applied to remap the extrapolated data back to the original coordinate system. The method appears to be extremely accurate, with 2D impulse responses and poststack migration results from the 2D SEG/EAGE salt model rivalling or exceeding the fidelity of generalized screen propagators (de Hoop et al, 2000). Unfortunately, it is not obvious that the simple coordinate-stretching VACT-transform suitable for 2D can be extended to 3D with the same accuracy.

EXTRAPOLATOR COMPARISON

A simple 2D synthetic was designed to show the differences between the five extrapolators (PSPI, NSPS, SNPS, Weyl, and PAVG). The results are shown in Figure 3. In Figure 3a two impulses are input at time 1s and propagated 200m through a 2D media with a vertical velocity step from 2000m/s (left) to 3000m/s (right). The exact two-way response is shown in Figure 3b. A good one-way extrapolator should approximate closely the following key features: first, the wavefield remains continuous at the step boundary, and second, it refracts to lower velocity (left) and higher velocity (right) as it crosses the boundary.

Figure 3c illustrates how PSPI uses the velocity at the output point to determine the traveltimes from each input to output point, for both the space-frequency (Kirchhoff) and wavenumber-frequency domain implementations. The extrapolator response is shown in Figure 3d. Notice that the desired response is not observed. Although the wavefield has the correct refractive slope, it is discontinuous at the boundary. The response of the wavenumber-frequency domain PSPI implementation is shown in Figure 3e. The result is almost identical, except for spatial wraparound that is somewhat attenuated by using a complex velocity.

Figure 3f illustrates how NSPS uses the velocity at the input points to determine the traveltimes from each input to output point. The extrapolator response is shown in Figure 3g. The desired response is not obtained, although the response obtained differs from the PSPI response. With NSPS, the wavefield is continuous at the boundary but has the incorrect refractive slope. The response of the wavenumber-frequency domain NSPS implementation is shown in Figure 3h. The result is almost identical to the space-frequency domain NSPS result, except for spatial wraparound that is, again, somewhat attenuated by using a complex velocity.

Figure 3i illustrates how SNPS is a cascade of PSPI followed by NSPS (or NSPS/PSPI). For a large step size like the 200m step used here, two wavefields appear at the boundary. For smaller step sizes SNPS can be shown to be more stable than either PSPI or NSPS. Only the wavenumber-frequency domain SNPS result is shown here. The space-frequency domain SNPS implementation is similar, but without the wraparound.

Figure 3k illustrates how the Weyl extrapolator uses an average of the input and output velocities. As might be expected, the response (Figure 3l) is a combination of a smaller discontinuity (compared with PSPI), and a less incorrect refractive slope (compared with NSPS).

Figure 3m illustrates how the new Kirchhoff PAVG extrapolator uses an estimate of the average slowness along the straight-ray travel path from each input to output point. The extrapolator response is shown in Figure 3n. The wavefield is continuous at the boundary and the refractive slope is close to the exact desired response. For comparison, Figure 3o is a repeat of the exact result given previously in Figure 3b.

In 2D, the average slowness along each ray path can be easily calculated as a difference between integrated slownesses. The multiple directions introduced in 3D complicate this simple approach. We have yet to implement an algorithm for estimation of 3D average-slowness, but plan to use a combination of fine grids near the input and output points with coarse grids in between.

TOWARDS ACCURATE IMAGING IN DEPTH

In this section, we examine four important considerations for accurate imaging in depth: 1) accurate extrapolators, 2) accurate shot modeling including amplitude effects of shot arrays, ghosting and near surface multiple effects, and near-surface variable velocity subsurface; 3) careful preprocessing of the shot-record to achieve a maximum bandwidth zero-phase wavelet with no time delay; and 4) a phase and amplitude stable imaging

condition. Kelly and Ren (2003) identify a fifth consideration that we do not address here: 5) conservation of vertical energy flux. We plan to investigate this for future implementations. The accuracy of extrapolators has been discussed in the previous section, where we suggest that a slowness averaged Kirchhoff extrapolator has phase closest to the ideal exact extrapolator, so we continue with considerations 2) through 4).

For ‘true-amplitude’ or ‘relative-amplitude-preserving’ wave-equation depth migration, we seed the source function (including array effects) at depth using analytic Green’s functions. Unfortunately, it is difficult to incorporate short-period near surface multiples into the analytic Green’s functions. Instead, their effects are mitigated by preprocessing, or incorporated into the source wavelet. However, array effects might remain that result in inaccurate source modeling. Hopefully, these effects are reduced to the same level as other approximations inherent in depth imaging. Figure 4a show how analytic Green’s functions might be used to seed the source wavefield at depth $2dz$. The source array is composed of monopoles with ghosting. The subsurface is constant velocity to the depth of the water. Figure 4b illustrates a more complicated situation that might arise with land data. The source array is composed of dipoles distributed over topography. In this case, the subsurface is variable velocity. Kelly and Ren (2003) suggest seeding such a source to a depth at a constant velocity representative of the near source, backward extrapolating the seeded source wavefield to the source location using the same constant velocity, then forward extrapolating through the variable velocity medium. Their tests suggest that this produces a good estimate of the forward extrapolated wavefield. We intend to test this concept against finite difference models.

Figure 5 is an example a source wavefield for the Marmousi dataset, seeded at a depth of 24m as a zero-phase wavelet using analytic constant velocity Green’s functions, one for each of the sources and ghosted sources in Figure 4a. The upper portion of the wavelet in Figure 5a is wrapped in time. To optimize focusing, the 24 Hz zero-phase Ricker wavelet has been chosen to match the preprocessed data (see Figure 6). After propagation to 400m (Figure 5b), the wavefield is effectively zero-phase, but now includes amplitude variations and phase delays arising from propagation through the variable velocity Marmousi model.

Finite difference modeling of the Marmousi near surface was used to get a good estimate of the effects of the source and receiver arrays, ghosting, and waterbottom multiples on the recorded wavelet (see Geiger and Daley, 2003). These effects cannot be easily accounted for using one-way propagators. Figure 6 shows how the input airgun wavelet (left) is modified by these effects. The resulting wavelets (right – one for normal incidence and one for 45° incidence) can be closely approximated by a zero-phase wavelet with a 60ms time delay. Figure 7 shows the results from finite difference modeling of an isolated Marmousi reflection event, before (left) and after (right) gap deconvolution with a 40ms gap and 200ms operator. A zero-phase whitening has also been applied.

For optimal imaging, it is essential that the modeled source and the processed data are zero-phase and matched in bandwidth. Residual time delays or time advances on either side can lead to poor focusing and inaccurate imaging. In Figure 8 (left), excellent focusing is achieved for a point diffractor at $x=0$, $z=200$. The majority of the energy is

well focused at the desired image point, although a low clip value has been chosen to show migration and aperture artifacts. In Figure 8 (right), a 60ms time delay has been introduced into the receiver wavefield. It would be tempting to correct the ‘smile’ by adjusting the migration velocity model.

The final piece of the puzzle is a good imaging condition. Following Zhang et al. (2002), we estimate reflectivity at each depth point using a cross-correlation of the downward continued source and receiver wavefields divided by an autocorrelation of the downward continued source wavefield. This stabilizes the phase of the estimator. Instead of a stability factor in the denominator, a mute is applied to the extrapolated wavefields based on a percentage of the total source energy at that depth level. This appears to do a good job of removing large estimates of reflectivity that arise when the source amplitude is small, and introduces less error than a stability factor. Kelly and Ren (2003) suggest a variety of other approaches that need to be tested against our approach. Our brief experience is that the dynamic mute produces excellent images. Further tests are required to examine the relative amplitude preserving characteristics of our approach.

IMAGES OF MARMOUSI

A shallow portion of the Marmousi model was chosen to test our approach to imaging (Figure 9). Although this portion contains a strong velocity contrast, multiple arrivals and wavefield refraction are minimal. Thus, it is not the ideal portion of the data to test our slowness averaged extrapolator. However, at these shallow depths ($\leq 400\text{m}$) the relatively long offsets ($\leq 2575\text{m}$) result in high angles of wavefield propagation (see Figure 9d). As per the discussions in the previous section, the shots are seeded within the water layer at 24m depth using analytic Green’s functions corresponding to an array of ghosted monopoles, each shot-record is preprocessed with a gap decon and static shift, and the two wavefields are imaged at depth after propagation using a crosscorrelation over autocorrelation imaging condition with stability mute. Each image is created as an unweighted sum of 49 prestack migrated shot records. The only difference between the various images is the type of extrapolator.

Figure 9b is a Marmousi depth migration image using Kirchhoff PAVG (slowness-averaged) extrapolator with 90° operator aperture (survey aperture bounded over distance 4000m-5500m – no edge taper). Figure 9c is a Marmousi depth migration image using a Kirchhoff PSPI-type extrapolator with 90° aperture. The PAVG extrapolator appears to produce a slightly better image, with better continuity along the bright reflector on the right hand side, fewer artifacts to the upper right of the central bright reflector, and slightly better focusing of the small reflectivity steps in the shallow dipping events.

Figure 9e is a Marmousi depth migration image using Kirchhoff PAVG (slowness-averaged) extrapolator with 84.5° operator aperture with 1.75° taper (survey aperture bounded by distance 4000m-5500m – no edge taper), corresponding to a 31 sample convolution operator ($10\text{dx}/5\text{dx}$ taper per dz each side). Steeper dips are not image correctly (circled). In a companion paper (Liu et al. 2003) we introduce a adaptive taper that should reduce the artifacts and errors associated with limited aperture extrapolators. The adaptive taper extrapolators are currently being tested as part of Kun Liu’s MSC thesis research.

CONCLUSIONS

In simple synthetic tests, the slowness-averaged (PAVG) Kirchhoff extrapolator exhibits superior phase behaviour compared with PSPI, NSPS, SNPS or Weyl extrapolators. For true amplitude imaging, the accuracy of the extrapolator is only one of many important factors. We address three additional factors: accurate preprocessing, source modeling, and the migration imaging condition. Initial results imaging the shallow portion of the Marmousi dataset suggest that the PAVG extrapolator is indeed the most accurate, but that careful attention needs to be paid to aperture tapering.

REFERENCES

- De Hoop, M.V., Le Rousseau, J.H., and Wu, R.S., 2000, Generalization of the phase-screen approximation for scattering of acoustic wave: *Wave Motion*, **31**, 43-70.
- Gazdag, J. 1978, Wave equation migration with the phase-shift method: *Geophysics*, **43**: 1342-1351.
- Geiger, H.D. and Daley, P.F. Finite difference modelling of the full acoustic wave equation in Matlab: CREWES Research Report **15**.
- Geiger, H.D., Margrave, G.F., Foltinek, D.S, Langlois, J.M., 2002, Parallel 3D prestack depth migration using recursive Kirchhoff extrapolation: CREWES Research Report, **14**
- Kelly, S., and Ren, J., 2003, Key elements in the recovery of relative amplitudes for shot record migration, *Ann. Internat. Mtg: Soc. of Expl. Geophys. Expanded Abstracts MIG P1.5*
- Liu, K., Geiger, H.D., and Bancroft, J.C., 2003, Tapering in the wavefield extrapolation: CREWES Research Report, **15**.
- Margrave, G.F., and Daley, P.F., 2001, Recursive Kirchhoff extrapolators, CREWES Research Report, **13**.
- Margrave, G.F., and Geiger, H.D. 2002, Wavefield resampling during Kirchhoff extrapolation: CREWES Research Report, **14**
- Margrave, G.F., and Ferguson, R.J., 1998, Explicit Fourier wavefield extrapolators: 10th Annual CREWES Research Report.
- Margrave, G. F. and Ferguson, R. J., 1999, Wavefield extrapolation by nonstationary phase shift: *Geophysics*, **64**, 1067-1078.
- Ferguson, R.J., and Margrave, 2001, Prestack depth imaging by symmetric nonstationary phase shift: *Geophysics*, **67**, 594-603.
- Weyl, H., 1931, *The Theory of Groups and Quantum Mechanics*: Dover edition (pub 1950).
- Xu, S. Jin, S., and Ma, Z., 2003, One-way wavefield extrapolation via velocity adaptive coordinate transform, 73rd Ann. Internat. Mtg: Soc. of Expl. Geophys. Expanded Abstracts, MIG-7.1.
- Zhang, Y, Sun, J.C. and Gray, S.H., 2003, Aliasing in wavefield extrapolation prestack migration: *Geophysics* **68**, 629-633.

FIGURES

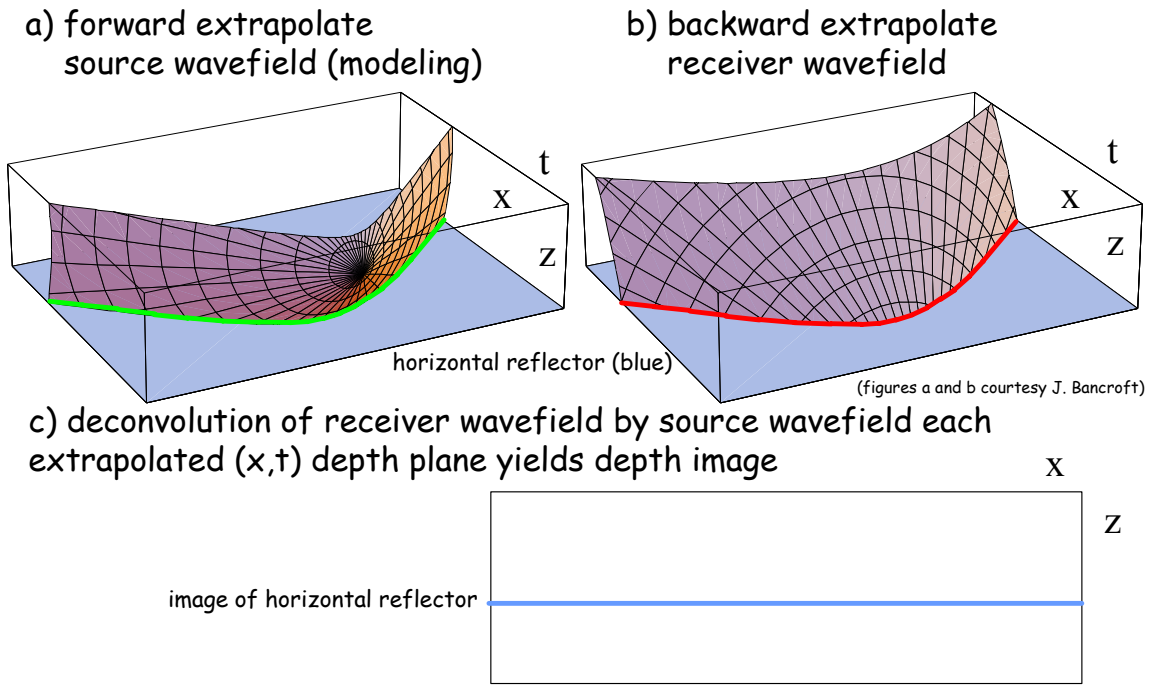


FIG. 1:a-c) Wave equation depth migration = wavefield extrapolation + imaging condition.

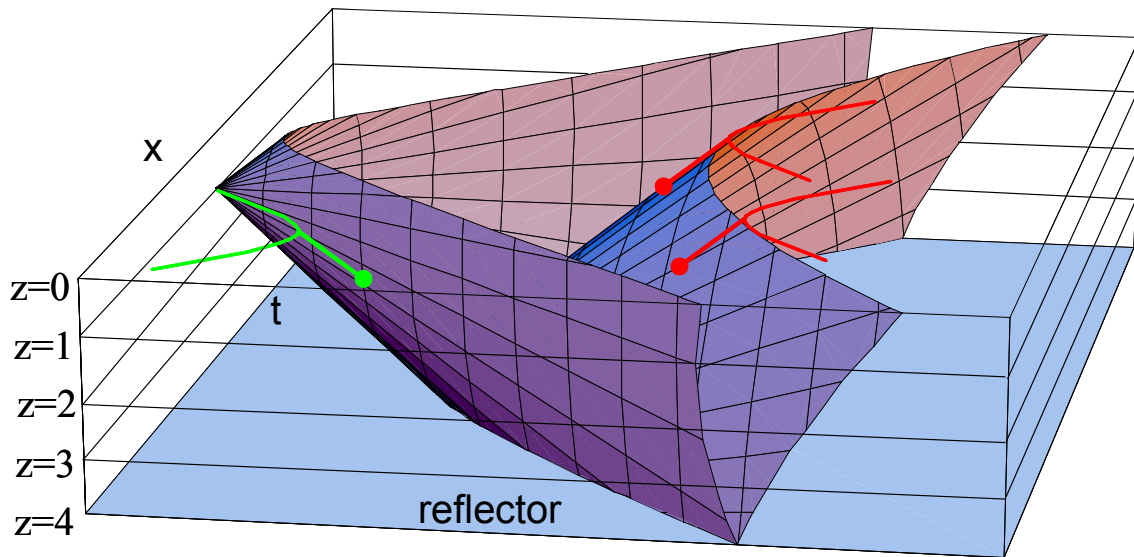


FIG. 2: In constant velocity, 2D forward (light) and backward (dark) extrapolators sum over a hyperbola and output to a point. The extrapolators do not vary with time, and thus can be implemented efficiently in the space-frequency domain.

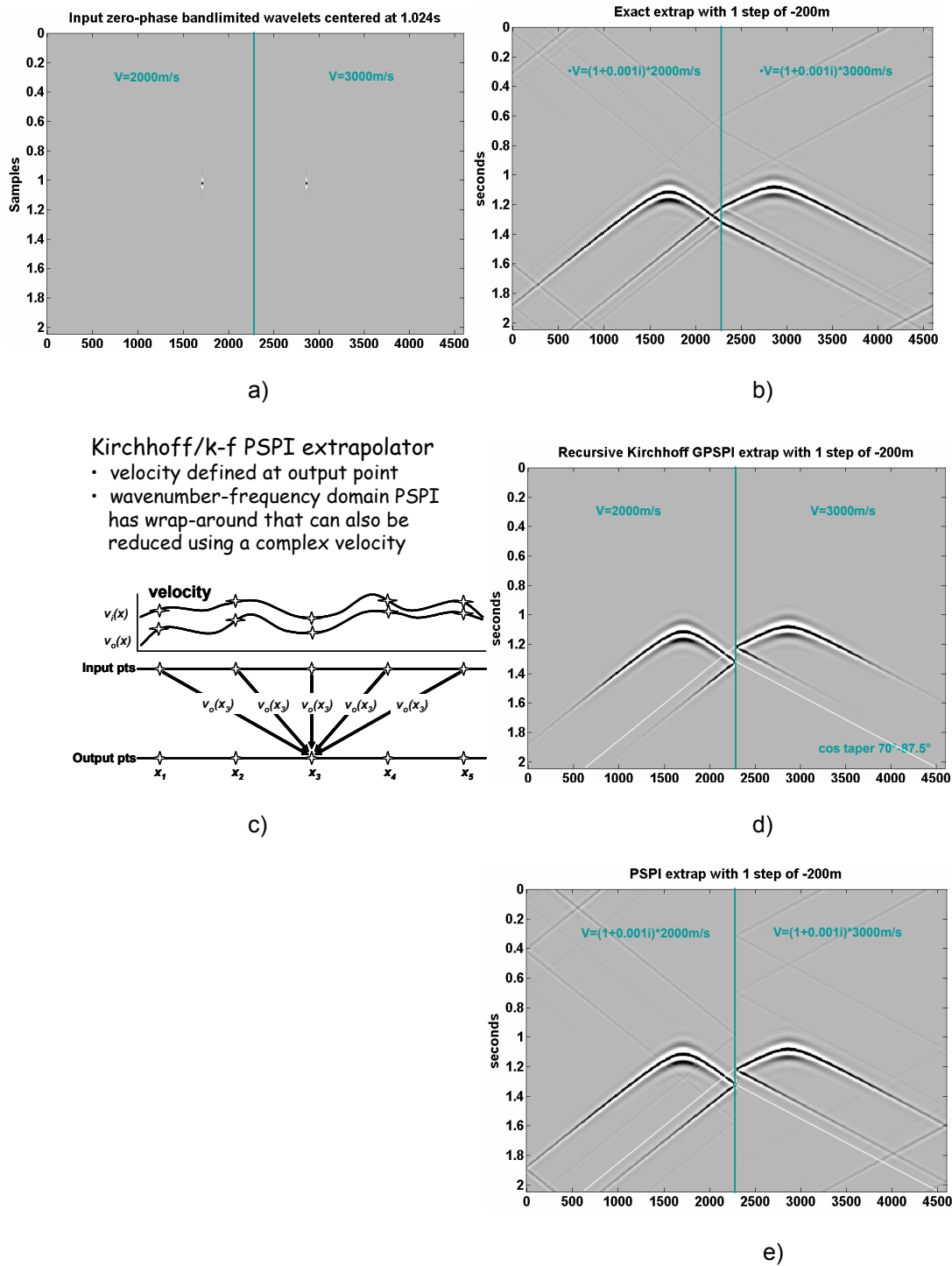
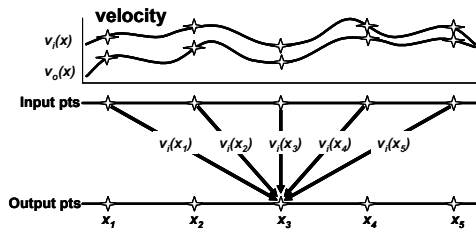


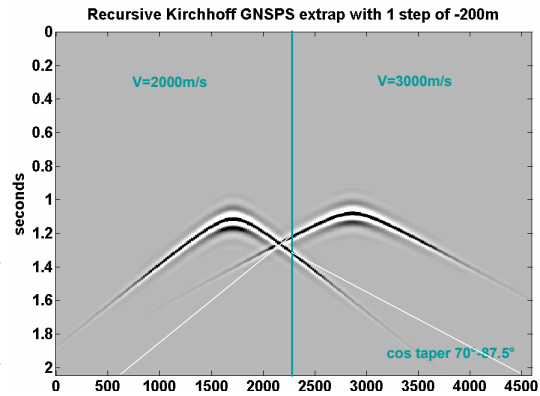
FIG. 3:a) Two impulses are input at time 1s and propagated 200m through a media with a velocity step from 2000m/s (left) to 3000m/s (right). b) The exact two-way response shows the key features that a good one-way extrapolator should approximate closely: the wavefield is continuous at the step boundary, and refracts to lower velocity (left) and higher velocity (right). Note: reflections are not expected with one-way extrapolators. c) PSPI uses the velocity at the output point to determine the traveltime from each input to output point, for both the space-frequency (Kirchhoff) and wavenumber-frequency domain implementations d) The wavefield is discontinuous at the boundary, but has the correct refractive slope. e) A wavenumber-frequency domain PSPI implementation with wraparound attenuated by using a complex velocity.

Kirchhoff/k-f NSPS extrapolator

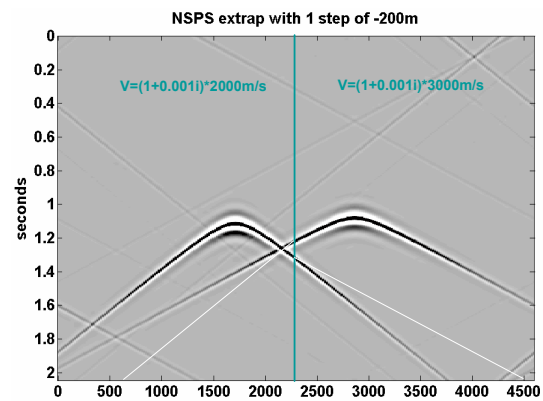
- velocity defined at input points
- wavenumber-frequency domain NSPS has wrap-around that can also be reduced using a complex velocity



f)



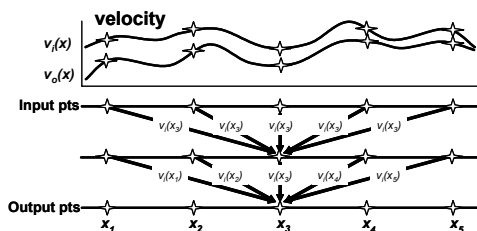
g)



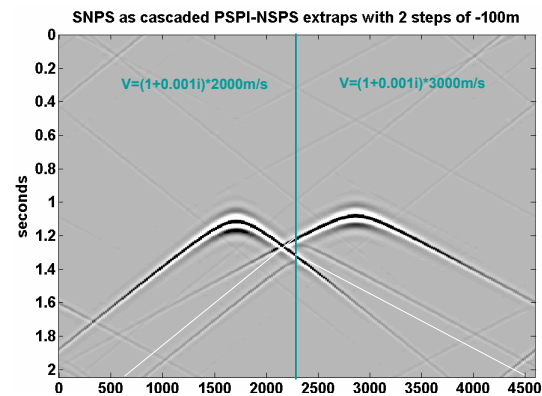
h)

SNPS as cascaded k-f PSPI/NSPS

- velocity defined using input points but output point formulation possible
- wavenumber-frequency domain SNPS has wraparound that can be reduced using complex velocities



i)

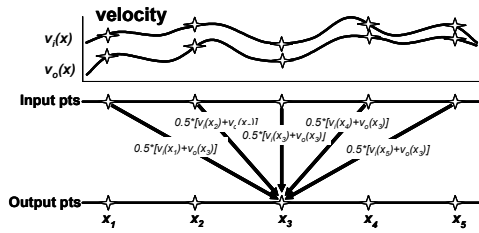


j)

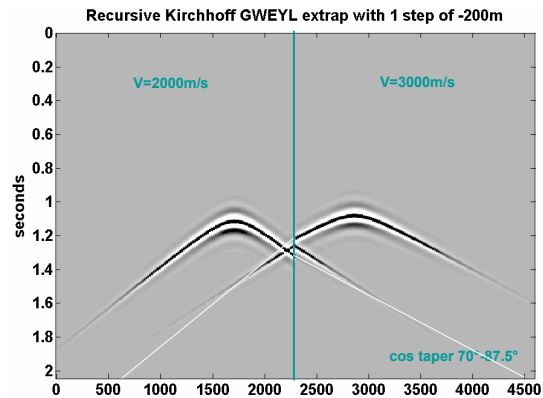
FIG. 3 (cont) f) NSPS uses the velocity at the input points to determine the traveltime from each input to output point. g) The wavefield is continuous at the boundary, but has the incorrect refractive slope. h) A wavenumber-frequency domain NSPS implementation with wraparound attenuated by using a complex velocity. i) SNPS is a cascade of PSPI followed by NSPS (or NSPS/PSPI). For a large step size like the 200m used here, two wavefields appear at the boundary. For smaller step sizes SNPS can be shown to be more stable than either PSPI or NSPS. Only the wavenumber-frequency domain SNPS result is shown here. The space-frequency domain SNPS implementation is similar, without the wraparound.

Kirchhoff WEYL extrapolator

- velocity defined as average of velocities at input and output points
- no wavenumber-frequency domain equivalent for Weyl extrapolator



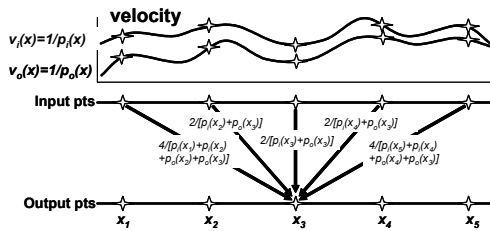
k)



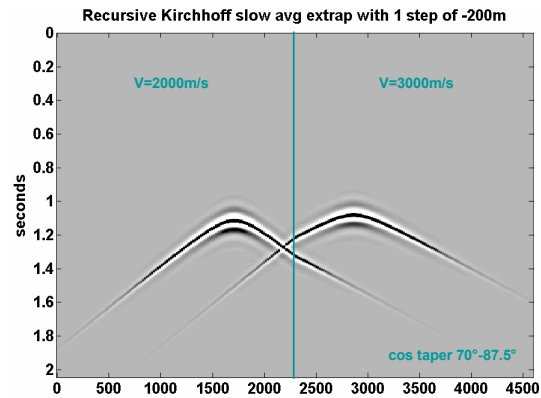
l)

Kirchhoff averaged slowness

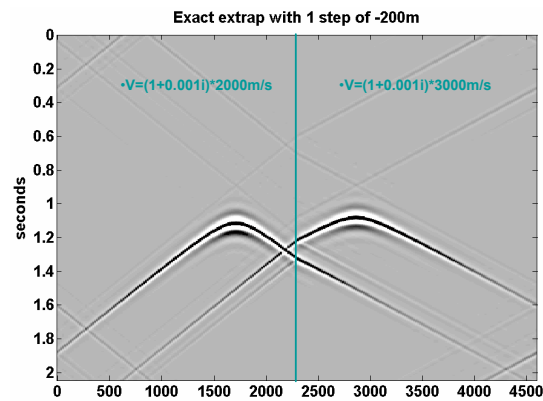
- velocity defined using average of slownesses along straight ray path
- **best performance of all extrapolators based on kinematics and amplitudes**



m)



o)



p)

FIG. 3 (cont) k) The Weyl extrapolator uses an average of the input and output velocities. l) As might be expected, the result is a combination of a smaller discontinuity (compared with PSPI), and a less incorrect refractive slope (compared with NSPS). m) The Kirchhoff PAVG extrapolator uses an estimate of the average slowness along the straight-ray travelpath from each input to output point. n) The wavefield is continuous at the boundary and the refractive slope is close to the exact desired response. o) The exact response from Figure 3b) shown again for comparison.

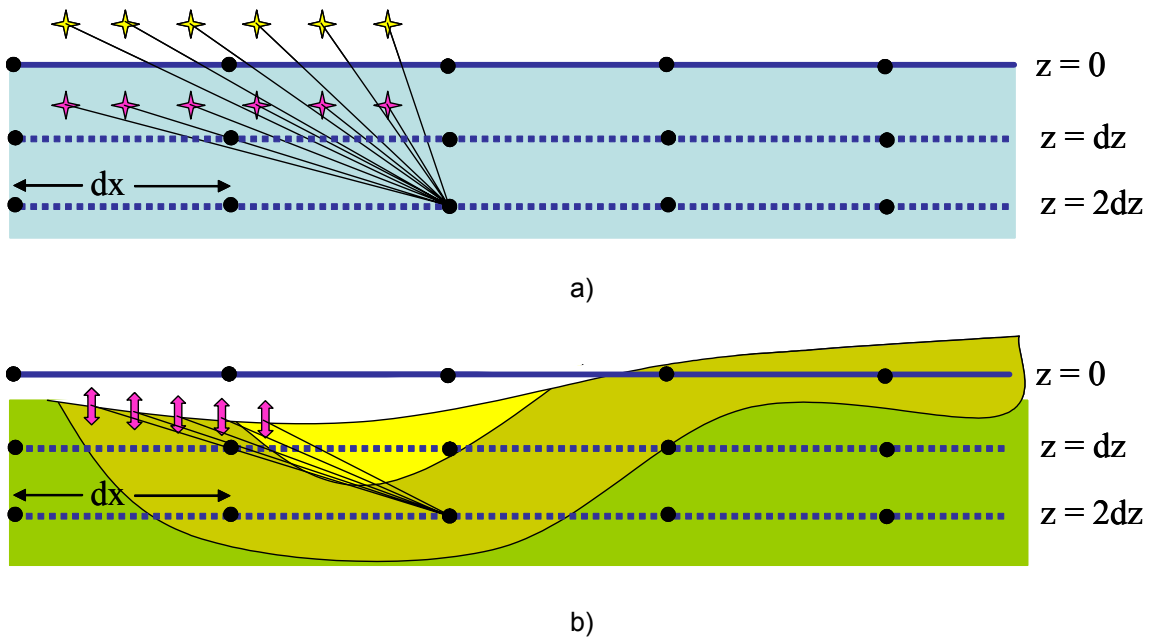


FIG. 4. For ‘true-amplitude’ or ‘relative-amplitude-preserving’ wave-equation depth migration, the source function (including array effects) is seeded at depth using analytic Green’s functions. a) A marine data example using a monopole array with ghosting and a constant velocity subsurface (to depth of water). b) A land data example using a dipole array with topography and a variable velocity subsurface.

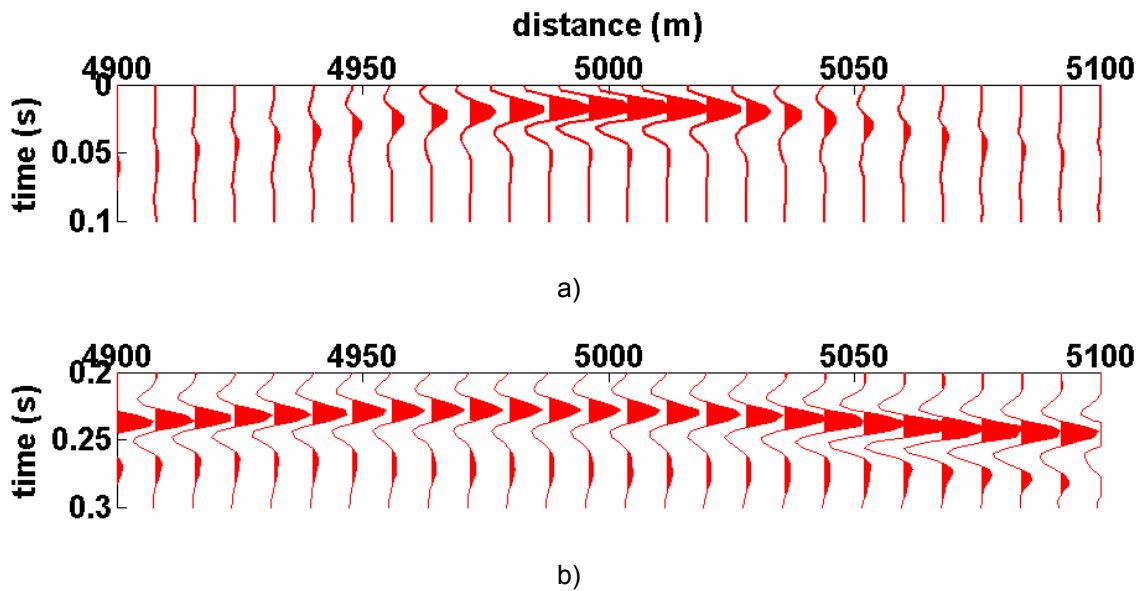


FIG. 5: An example source wavefield for the Marmousi dataset. a) The wavefield is seeded at a depth of 24m as a zero-phase wavelet using analytic constant velocity Green’s functions, one for each of the sources and ghosted sources in Figure 4a). The upper portion of the wavelet is wrapped in time. To optimize focusing, the 24 Hz zero-phase Ricker wavelet has been chosen to match the preprocessed data (see Figure 6). b) After propagation to 400m, the wavefield is effectively zero-phase, but now includes amplitude variations and phase delays arising from propagation through the variable velocity Marmouis model.

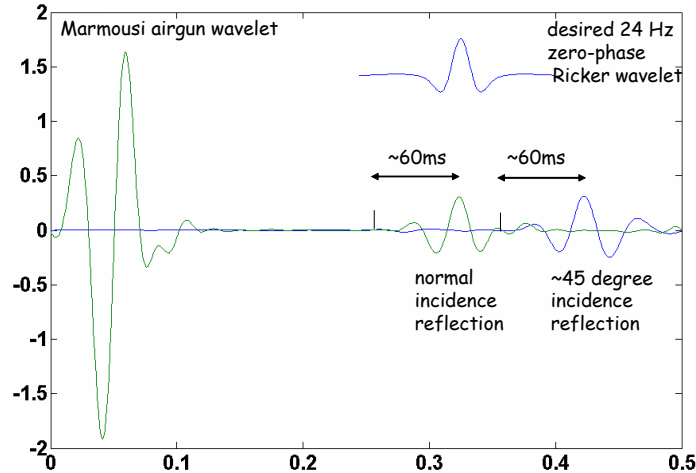


FIG. 6. The wavelet in the recorded data includes many effects, such as waterbottom multiples and ghosting, that cannot be easily accounted for using one-way propagators. For the Marmousi dataset, a finite difference model was used to determine how the input airgun wavelet (left) is modified by these effects. The resulting wavelet can be closely approximated by a zero-phase wavelet with a 60ms time delay. These observations guide the Marmousi preprocessing.

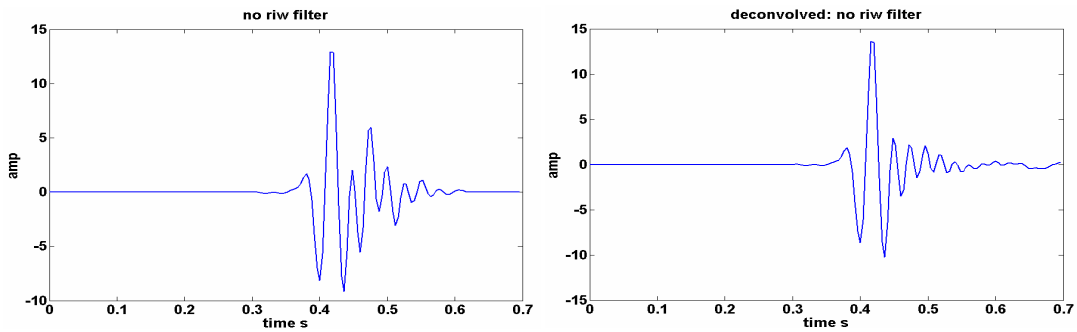


FIG. 7. Finite difference modeling of an isolated Marmousi reflection event, before (left) and after (right) gap deconvolution with a 40ms gap and 200ms operator. A zero-phase whitening has also been applied.

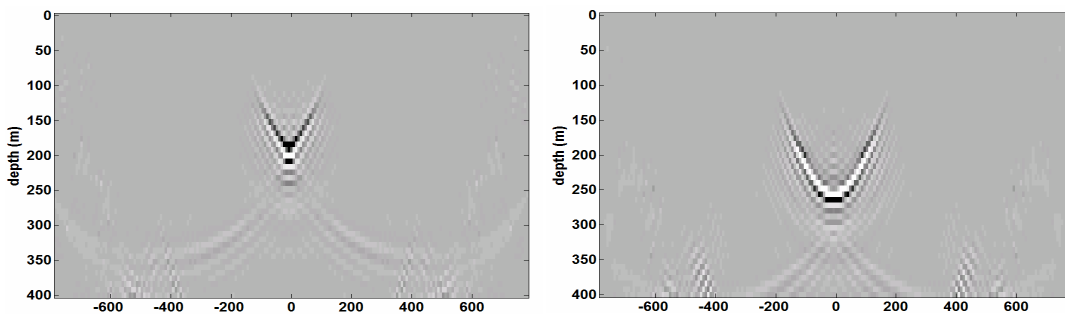


FIG. 8. Optimal imaging is obtained when both the source wavefield and the receiver wavefield are true zero-phase, without time delay errors. On the left, excellent focusing is achieved for a point diffractor at $x=0$, $z=200$ (the low clip value shows migration and aperture artifacts). On the right, a 60ms time delay has been introduced into the receiver wavefield. It would be tempting to correct the 'smile' by adjusting the migration velocity model.

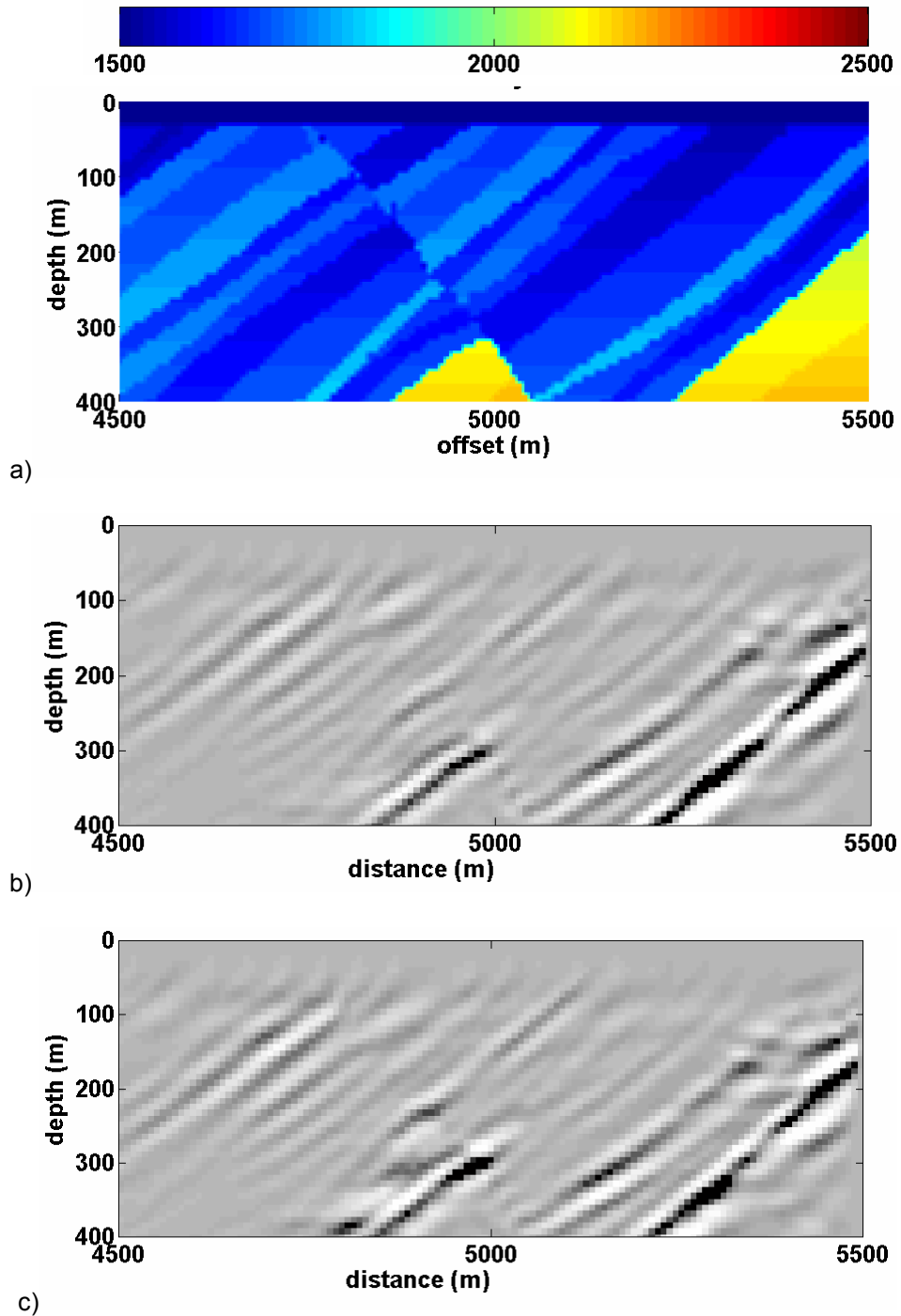


FIG. 9: a) Selected portion of upper 400m of the Marmousi velocity model. b) Marmousi depth migration image using Kirchhoff PAVG (slowness-averaged) extrapolator with 90° operator aperture (survey aperture bounded over distance 4000m-5500m – no edge taper). This and following figures an unweighted sum of 49 prestack migrated shot gathers, imaged with a stabilized deconvolution imaging condition. c) Marmousi depth migration image using a Kirchhoff PSPI-type extrapolator with 90° aperture.

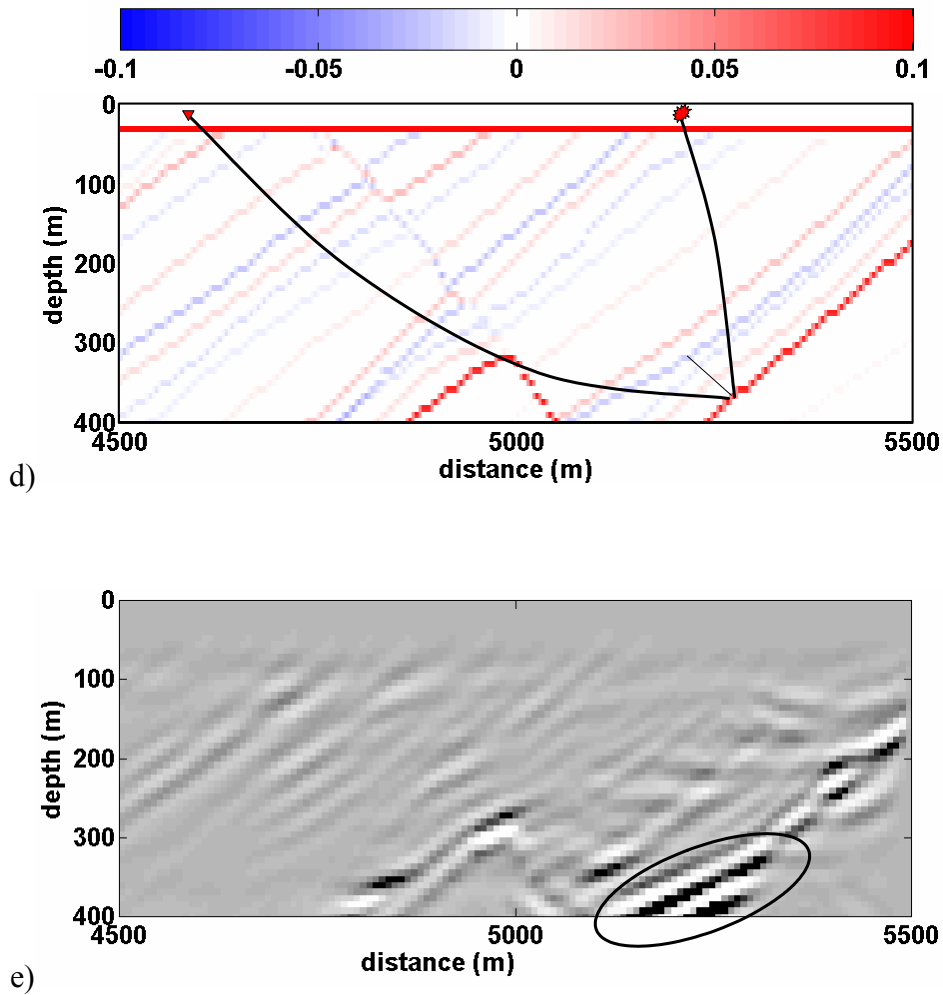


FIG. 9 (cont): d) Upper 400m portion of the Marmousi reflectivity model (same as 9a), calculated as zero-offset vertical incidence reflectivity. For prestack data, specular reflections off of a moderately steep dipping event can demand accurate high-angle wavefield propagation, as shown by a possible raypath from source to reflector to receiver. e) Marmousi depth migration image using Kirchhoff PAVG (slowness-averaged) extrapolator with 84.5° operator aperture with 1.75° taper (survey aperture bounded by distance 4000m-5500m – no edge taper), corresponding to a 31 sample convolution operator ($10dx/5dx$ taper per dz each side). Steeper dips are not image correctly (circled).